Coupling between diffusion and orientation of pentacene molecules on an organic surface

Paul Rotter[1], Barbara A. J. Lechner[2,3], Antonia Morherr[1], David M. Chisnall[2], David J. Ward[2], Andrew P. Jardine[2], John Ellis[2], William Allison[2], Bruno Eckhardt[1] and Gregor Witte[1*]

[1]Fachbereich Physik, Philipps-Universität Marburg, 35032 Marburg, Germany,

[2]Cavendish Laboratory, University of Cambridge, JJ Thomson Avenue, Cambridge CB3 0HE, United Kingdom,

[3]Present address: Materials Sciences Division, Lawrence Berkeley National Laboratory, Berkeley, CA 94720, USA.

[*]e-mail: gregor.witte@physik.uni-marburg.de

Nature Materials – http://dx.doi.org/10.1038/nmat4575

Received 7 August 2015; accepted 20 January 2016; published online 22 February 2016

The realization of efficient organic electronic devices requires the controlled preparation of molecular thin films and heterostructures. Since top-down structuring methods like lithography cannot be applied to van der Waals bound materials[1], surface diffusion becomes a structure-determining factor that requires microscopic understanding. Scanning probe techniques provide atomic resolution, but are limited to observations of slow movements and therefore constrained to low temperatures. In contrast, the helium-3 spin-echo (HeSE) technique achieves spatial and time resolution at the nm and ps scale, respectively, thus enabling measurements at elevated temperatures[2]. Here we use HeSE to unveil the intricate motion of pentacene admolecules diffusing on a chemisorbed monolayer of pentacene on Cu(110), that serves as a stable, well-ordered organic model surface[3]. We find that pentacene moves along rails parallel and perpendicular to the surface molecules. The experimental data is explained by admolecule rotation that enables a switching between diffusion directions, which extends our molecular level understanding of diffusion in complex organic systems.

Molecular diffusion controls the dynamics of chemical reactions and film growth processes[4] and is of fundamental importance to the emerging fields of organic electronics and molecular nanotechnology[5–8]. At present, microscopic characterization of diffusion is focused on motion of molecules chemisorbed on inorganic, mostly metallic, substrates as this facilitates the application of scanning tunnelling microscopy (STM)[9–11]. In contrast, virtually no experimental data are reported that directly probe molecular diffusion on molecular surfaces. As a consequence of the rather weak, essentially van der Waals, intermolecular interaction with the surface, admolecule motion at room temperature becomes too fast for observation by STM, which also carries the risk of tip-induced motion[12,13]. However, reducing the temperature may freeze out degrees of freedom (DOF), thereby suppressing potentially important diffusion paths. Unsurprisingly, the behaviour of molecules on organic surfaces is different from inorganic systems, because potential wells describing the interaction between aromatic admolecules and molecular solids are often less pronounced compared to adatoms or covalently bound adsorbates. Moreover, the interplay between rotational DOF and surface anisotropies creates complex potential energy landscapes so that dominant diffusion pathways do not immediately stand out.

Among the many π-conjugated molecules that are of interest for organic electronics, pentacene constitutes a well characterized reference system that serves as archetype for organic semiconductors and thin film growth[14]. It can be regarded as rigid, so that conformational DOF which would further complicate diffusion[15] do not have to be considered.

Although organic semiconductors offer the advantage of low temperature processing, crystalline organic surfaces often become disordered and already exhibit pre-melting at room temperature. To exclude these effects, we used a pentacene monolayer (ML) chemisorbed on Cu(110) giving a well-ordered and stable organic model surface[3] (Supplementary Fig. 1). A small coverage of pentacene admolecules diffuse on top of the overlayer, while the chemisorbed pentacene surface remains unchanged.

Pentacene admolecule diffusion was probed directly by HeSE, which detects a small energetic Doppler broadening of He atoms upon scattering from moving adparticles. However, the finite monochromaticity of a supersonic He atom beam limits the energy resolution and therefore the range of detectable diffusion rates[2]. To overcome this limitation, a concept from the well-established neutron spin-echo scattering is adopted[16]; the energy change is converted to a loss of ^{3}He atom spin polarization, as illustrated in Fig. 1a. The nuclear spin state of the incident ^{3}He is polarized and split into two coherent wave packets, which reach the sample with a time delay Δt (also called *spin-echo time*). After scattering, the wave packets are recombined and the resulting polarization is measured. If there is movement on the sample surface, the wave packets scatter differently and once recombined, reduce the final beam polarization. Because the process is based on self-interference of each ^{3}He atom, the polarization loss only depends on the change in energy and not the beam energy itself[2]. Since the impinging He atoms have very low kinetic energies (< 10 meV), they do not affect the observed motion, while the large He atom scattering cross section[17] gives outstanding sensitivity.

A HeSE measurement yields polarization as a function of Δt for a fixed surface parallel momentum transfer $\Delta \boldsymbol{K}$ (Fig. 1b). The polarization is proportional to the so-called intermediate scattering function $I(\Delta \boldsymbol{K}, \Delta t)$, which is related to the pair correlation function through a Fourier transform[18], and has been calculated analytically for various prototypical types of surface motion. Specifically, the

Chudley-Elliot model for particles hopping on a lattice predicts an exponentially decaying $I(\Delta \boldsymbol{K}, \Delta t)$ with increasing spin-echo time, Δt, where the decay constant (so-called dephasing rate) α vanishes when the momentum transfer $\Delta \boldsymbol{K}$ matches a reciprocal lattice vector and varies sinusoidally in between[19]. Generally, the shape of $\alpha(\Delta \boldsymbol{K})$ reflects the diffusion process and transition rates, while the temperature dependence $\alpha(T)$ reveals the energetic barriers. To determine $\alpha(\Delta \boldsymbol{K})$ experimentally, HeSE measurements were acquired for a range of $\Delta \boldsymbol{K}$ values along a selected azimuth by systematically varying the angle of incidence γ (see Fig. 1a) and extracting the dephasing rate α from the resulting exponentials' decays (Fig. 1b).

As a consequence of the conservation of momentum, only motion projected onto the specific azimuthal direction is detected, defined by the scattering plane via the azimuthal angle, ϕ (Fig. 1a green arrow). Since the pentacene molecules in our model surface are uniformly oriented within a rectangular unit cell, as illustrated in Fig. 1, we anticipate perpendicular modes of diffusion. Thus we can take advantage of the directional sensitivity of HeSE by performing measurements along the high-symmetry azimuthal directions.

The principal $\alpha(\Delta \boldsymbol{K})$ curves for pentacene diffusing on a pentacene monolayer, shown in Fig. 2, exhibit distinct minima at $|\Delta \boldsymbol{K}| = 0.38$ Å^{-1} and 0.87 Å^{-1} along [1-10] and [001], respectively, which agree perfectly with the corresponding diffraction pattern[3] of the pentacene surface lattice (Fig. 2 inset). These minima do not arise from diffraction at immobile surface molecules because our analysis of dephasing rates is only sensitive to aperiodic motion, such as diffusion. In particular, static molecules or islands that could be attached to surface defects, do not contribute to the detected dephasing signal. The fact is experimentally corroborated by complementary HeSE measurements that were recorded at a larger coverage of 0.44 ML pentacene admolecules, yielding a very similar $\alpha(\Delta \boldsymbol{K})$ curve (Supplementary Fig. 2). Therefore, the minima are a clear indication that admolecules reside at specific sites that have the symmetry of the underlying pentacene surface corrugation. For hopping between those sites, a sinusoidal $\alpha(\Delta \boldsymbol{K})$ dependence is expected. However, a closer inspection of the measured $\alpha(\Delta \boldsymbol{K})$ curve, especially along the [001] azimuth (Fig. 2 lhs), reveals that the maxima are wider and the minima narrower than expected for hops between adjacent sites (compare with grey dashed lines). Such behaviour has been

observed for long jumps of adsorbates in the low-friction regime[20], where admolecules keep their kinetic energy long enough to overcome several diffusion barriers at once. In contrast, recent diffusion studies[21] revealed a high friction coefficient, η, for benzene and other small aromatic molecules, which was later attributed to their rotational DOF[22]. For large molecules like pentacene, the friction is expected to be even higher. Thus the question arises as to which microscopic diffusion pathways cause the deviation from a sinusoidal shape.

As a scattering technique, HeSE provides detailed ensemble properties of adparticle motion. Information about individual diffusion processes, such as the energy barriers and friction, can be extracted by Langevin computer simulation of trajectories that are transformed into the intermediate scattering function for comparison with the experimental polarization curves. However, such simulations require a potential energy surface (PES), which describes the interaction between admolecule and substrate. For covalently bound or small chemisorbed adparticles, a parametrized PES can be constructed using surface geometry and density functional theory (DFT) calculations[23,24]. However, the limited computational precision of DFT methods for purely van der Waals interacting systems means such predictions are still challenging[25].

To obtain an *a priori* PES, we describe the forces between the immobile pentacene molecules (within the well-defined surface lattice) and the diffusing pentacene using the MM3 force field[26] which has been shown to represent the interactions between organic molecules realistically[25]. In its minimum energy configuration the admolecule lies flat, with its long axis aligned either parallel or perpendicular to the surface molecules. Therefore, azimuthal rotation is needed for a transition between the two minima and we determine the potential energy as a function of lateral admolecule position and its azimuthal orientation (see Supplementary Section 5). The resulting PES is used in Langevin simulations at 300 K which yields reasonable agreement with the experiment (Supplementary Figs. 3–4). To identify the most important features of the PES, we use a Fourier approximation (Supplementary Figs. 5–6, Table 1). This approach allows us to optimize the PES systematically and capture the essential surface dynamics needed to reproduce the experimental data, shown by the blue dots in Fig. 2 (details in Supplementary Fig. 7 and Table 2).

The optimized PES isosurfaces in Fig. 3a show effective rails which guide the admolecule

diffusion. Sideways diffusion without molecular rotation is suppressed by a barrier exceeding 185 meV, whereas the potential energy required for rotating the pentacene long axis is 110 meV at most. Figure 3b illustrates the resulting surface diffusion: an admolecule diffuses along a rail until the rotation barrier is overcome and it rotates by 90°. This *derailing* stops movement along the rail until the next rotation which *rerails* the admolecule. During this interval the molecule is free to move along the perpendicular rail, which can be well seen in the trajectory (for animation see Supplementary Movie 1). The decomposition of movement into those elementary processes is illustrated in Fig. 3c.

The maxima in the $\alpha(\Delta \boldsymbol{K})$ curve depend on the rotation barrier and temperature dependent simulations yield an effective activation energy of 85 ± 1 meV along [1-10], in good agreement with the value of 93 ± 9 meV determined by an Arrhenius analysis of the experimental data (Fig. 2 inset). The effective barrier of 101 ± 1 meV along [001] agrees with complementary higher coverage measurements (96 ± 8 meV, Supplementary Figure 2) and matches the expected increase due to the *derailing* barrier asymmetry, caused by a 25 meV elevation of the [1-10] rail w.r.t. [001]. The differences between the Arrhenius energies and the PES barriers are an expected consequence of the high friction and temperature[2]. Although we have clearly identified the pivotal role of the *derailing* process, we note that rotation itself was not detected directly through the HeSE analysis. The process was distinguished through the combination of elementary processes giving rise to apparent long jumps, as illustrated in Fig. 3d. Fast movement along a rail between *derailing* and *rerailing* appears as a long jump when projected onto that rail. The observed motion does not correspond to the fast movement along a rail but reflects the correlated recurrence of *derailing* stops that appear as jumps. Note that this explanation holds for both directions and results in the coincident minima in the experimental and simulated $\alpha(\Delta \boldsymbol{K})$ curves (Fig. 2), since the rails form a grid with the symmetry of the underlying surface. The interaction of shape anisotropic admolecules with anisotropic surfaces causes a peculiar coupling of diffusion directions which goes beyond anisotropic diffusion as reported previously e.g. for C_{60} on pentacene[27]. We obtained a Langevin friction coefficient of η = (1.8 ± 0.2) ps^{-1} which should be considered as a lower bound because some DOF were effectively frozen.

Based on the microscopic explanation of pentacene diffusion, an analytical model for hopping on a lattice with non-equivalent sites[28] was extended to account for admolecule orientation. The characteristics of the resulting $\alpha(\Delta \boldsymbol{K})$ curve, shown as solid black lines in Fig. 2, can then be mapped unambiguously to the microscopic processes. The model confirms that the rotation frequency determines the maximum dephasing rate. The speed of movement in-between orientation changes controls the length distribution of apparent long jumps and therefore determines the deviation from a sinusoidal shape. Real-space analysis of simulated trajectories at 300 K yields 26% double and 15% triple jumps along [001] direction ([1-10]: 16%, 2.6%) and tracer diffusion coefficients of 0.33 $Å^2ps^{-1}$ and 0.20 $Å^2ps^{-1}$ along the [001] and [1-10] azimuth, respectively. Since the [001] rail is energetically favoured and the spatial distance between possible *derailing* sites is shorter along this direction, the corresponding long jumps are more frequent and the $\alpha(\Delta \boldsymbol{K})$ curve broadening is more pronounced (Fig. 2). Hence, we confirm the intricate diffusion process where the azimuthal orientation of admolecules is responsible for the observation of long jumps.

In summary, we present the first observation of molecular scale diffusion in complex organic systems at room temperature. Diffusion of pentacene molecules on a pentacene surface highlights the pivotal role of molecular orientation, which leads to unexpected diffusion dynamics. Our findings enable a direct experimental validation of a PES constructed from force field schemes and will serve as an important benchmark for future *ab initio* approaches. Our results show how diffusive motion is linked to molecular orientation and substrate structure, which is of great importance for the emerging field of nanotechnology where functional molecular nanostructures are built using a bottom-up approach.

Acknowledgements

The authors acknowledge financial support from the EPSRC (EP/E0049621, B.A.J.L., D.J.W., D.M.C., W.A., A.P.J., J.E.), the Austrian Academy of Sciences (B.A.J.L.), the Royal Society (A.P.J.), the E.U. ERASMUS programme (A.M.) and the Deutsche Forschungsgemeinschaft (GRK 1782, P.R.). Underlying data are available at the University of Cambridge data repository (https://www.repository.cam.ac.uk/handle/1810/253563).

Author contributions

G.W. initiated the project. G.W., W.A. and A.P.J. planned the experiment. A.M., B.A.J.L., D.M.C. and D.J.W. performed the HeSE measurements. A.M., P.R., B.A.J.L. and J.E. analysed the data. P.R. ran the simulations. P.R. and B.E. developed the model. P.R., G.W., B.A.J.L. and B.E. wrote the manuscript.

Additional information

Supplementary information is available in the online version of the paper at http://dx.doi.org/10.1038/nmat4575.

Correspondence and requests for materials should be addressed to G.W.

Competing financial interests

The authors declare no competing financial interests.

References

1. Forrest, S. R. The path to ubiquitous and low-cost organic electronic appliances on plastic. *Nature* **428,** 911–918 (2004).

2. Jardine, A. P., Hedgeland, H., Alexandrowicz, G., Allison, W. & Ellis, J. Helium-3 spin-echo: Principles and application to dynamics at surfaces. *Prog. Surf. Sci.* **84,** 323–379 (2009).

3. Söhnchen, S., Lukas, S. & Witte, G. Epitaxial growth of pentacene films on Cu(110). *J. Chem. Phys.* **121,** 525-534 (2004).

4. Barth, J. V. Transport of adsorbates at metal surfaces: from thermal migration to hot precursors. *Surf. Sci. Rep.* **40,** 75–149 (2000).

5. Dimitrakopoulos, C. D. & Malenfant, P. R. L. Organic Thin Film Transistors for Large Area Electronics. *Adv. Mater.* **14,** 99–117 (2002).

6. O'Neill, M. & Kelly, S. M. Ordered Materials for Organic Electronics and Photonics. *Adv. Mater.* **23,** 566–584 (2011).

7. Sarikaya, M., Tamerler, C., Jen, A. K.-Y., Schulten, K. & Baneyx, F. Molecular biomimetics: nanotechnology through biology. *Nat. Mater.* **2,** 577–585 (2003).

8. Grimsdale, A. C. & Müllen, K. The Chemistry of Organic Nanomaterials. *Angew. Chemie Int. Ed.* **44,** 5592–5629 (2005).

9. Otero, R. *et al.* Lock-and-key effect in the surface diffusion of large organic molecules probed by STM. *Nat. Mater.* **3,** 779–782 (2004).

10. Bartels, L., Wang, F., Möller, D., Knoesel, E. & Heinz, T. F. Real-Space Observation of Molecular Motion Induced by Femtosecond Laser Pulses. *Science* **305,** 648–651 (2004).

11. Wong, K. L. *et al.* A Molecule Carrier. *Science* **315,** 1391–1393 (2007).

12. Komeda, T., Kim, Y., Kawai, M., Persson, B. N. J. & Ueba, H. Lateral Hopping of Molecules Induced by Excitation of Internal Vibration Mode. *Science* **295,** 2055–2058 (2002).

13. Kim, Y., Motobayashi, K., Frederiksen, T., Ueba, H. & Kawai, M. Action spectroscopy for single-molecule reactions – Experiments and theory. *Prog. Surf. Sci.* **90,** 85–143 (2015).

14. Ruiz, R. *et al.* Pentacene Thin Film Growth. *Chem. Mater.* **16,** 4497–4508 (2004).

15. Hlawacek, G. *et al.* Characterization of Step-Edge Barriers in Organic Thin-Film Growth. *Science* **321,** 108–111 (2008).

16. Fouquet, P. *et al.* Measurements of molecule diffusion on surfaces using neutron and helium spin echo. *Physica B: Cond. Mat.* **385-386,** 269–271 (2006).

17. Poelsema, B. & Comsa, G. *Scattering of Thermal Energy Atoms*. **115,** (Springer Tracts in Modern Physics 115, Springer Berlin Heidelberg, 1989).

18. Van Hove, L. Correlations in Space and Time and Born Approximation Scattering in Systems of Interacting Particles. *Phys. Rev.* **95,** 249–262 (1954).

19. Chudley, C. T. & Elliott, R. J. Neutron Scattering from a Liquid on a Jump Diffusion Model. *Proc. Phys. Soc.* **77,** 353–361 (1961).

20. Ellis, J. & Toennies, J. P. Observation of jump diffusion of isolated sodium atoms on a Cu(001) surface by helium atom scattering. *Phys. Rev. Lett.* **70,** 2118–2121 (1993).

21. Hedgeland, H. *et al.* Measurement of single-molecule frictional dissipation in a prototypical nanoscale system. *Nat. Phys.* **5,** 561–564 (2009).

22. de Wijn, A. S. Internal degrees of freedom and transport of benzene on graphite. *Phys. Rev. E* **84,** 011610 (2011).

23. Lechner, B. A. J. *et al.* Atomic scale friction of molecular adsorbates during diffusion. *J. Chem. Phys.* **138,** 194710 (2013).

24. Lechner, B. A. J. *et al.* Jumping, Rotating, and Flapping: The Atomic-Scale Motion of Thiophene on Cu(111). *J. Phys. Chem. Lett.* **4,** 1953–1958 (2013).

25. Clancy, P. Application of Molecular Simulation Techniques to the Study of Factors Affecting the Thin-Film Morphology of Small-Molecule Organic Semiconductors. *Chem. Mater.* **23,** 522–543 (2011).

26. Allinger, N. L., Yuh, Y. H. & Lii, J. H. Molecular mechanics. The MM3 force field for hydrocarbons. 1. *J. Am. Chem. Soc.* **111,** 8551–8566 (1989).

27. Cantrell, R. A., James, C. & Clancy, P. Computationally Derived Rules for Persistence of C60 Nanowires on Recumbent Pentacene Bilayers. *Langmuir* **27,** 9944–9954 (2011).

28. Tuddenham, F. E. *et al.* Lineshapes in quasi-elastic scattering from species hopping between non-equivalent surface sites. *Surf. Sci.* **604,** 1459–1475 (2010).

Methods

Experiment. A Cu(110) single crystal (Surface Preparation Laboratory, The Netherlands) was cleaned by Ar^+ sputtering and annealing to 800 K in a background pressure of 7×10^{-11} mbar. A specular helium reflectivity exceeding 30 % confirmed a clean and flat copper crystal. Sublimation-cleaned pentacene (Aldrich, purity >99%) was deposited onto the substrate by line-of-sight dosing, sublimating its powder from a resistively heated Knudsen cell. Monitoring the reflectivity during pentacene deposition revealed a clear peak upon completion of the first monolayer due to its high degree of order[3] and allowed us to determine the coverage of subsequently deposited pentacene[29]. Throughout this study, a coverage of 0.23 ML on top of the pentacene ML is used. The helium diffraction pattern of the highly ordered pentacene monolayer was utilized to align the sample azimuthally[3]. The pentacene ML could be recovered by heating the sample to 450 K to desorb pentacene exceeding coverages of 1 ML. Such a desorption step enables the deposition of a well-defined coverage of pentacene admolecules, without traces remaining from the monolayer preparation. HeSE measurements were performed with a beam energy of 8.2 meV along two crystal directions to map two-dimensional motion, along [001] and 9° off [1-10]. Details regarding the 9° offset from [1-10] are given in the Supplementary Section 2.

Calculations. MM3(2000) calculations were performed with version 7.1.3 of the TINKER software package[30]. Rigid pentacene molecules (moment of inertia 4686 g/mol Å^2 for rotation) were used to represent admolecule and surface. The potential energy was calculated for 100 × 50 × 36 points in the 16.6 Å × 7.23 Å × 180° unit cell (see Supplementary Section 5). The Langevin simulation calculated single admolecule trajectories in the parametrized PES (integration time step 2 fs, trajectory length 10^4 × 650 ps and sampling time 2.9 ps according to the experimental values, averaged over 96 runs, simulation temperature 300 K for the $\alpha(\Delta\boldsymbol{K})$ curve and 270–330 K in 10 K steps for the Arrhenius analysis; see Supplementary Section 4 for further details). The agreement of different coverage measurements justified the exclusion of interaction forces between admolecules (see Supplementary Section 3). Trajectories were transformed to the intermediate scattering function, treating the pentacene admolecules as point scatterers due to the large scattering cross section of He. As expected in the high friction regime, the overall diffusion constant

decreases with increasing η. Within the model framework, the effects of PES parameters and friction are assigned to distinct features in the experimental results (see Supplementary Section 6). Therefore, each parameter can only be changed slightly before a clear mismatch between simulated results and experiment emerges (even allowing for re-adjustment of the friction), which determines each parameter to within about 10%. The analytical model allows movement along the rails to be distinguished from another process that was termed the *derailing* correlation. The identification of this correlation complements the intermediate scattering function analysis, which only distinguishes different processes *a posteriori* based on separated time scales. For visualization of the analytical model the mean first passage time between derailing sites was determined to be 155 ps (57 ps) along [1-10] ([001]), and the mean residence time on the [1-10] ([001]) rail was 173 ps (350 ps), with less than 0.5% standard error of the mean (SEM) for all values. The relative SEM for the given long jump frequencies and diffusion coefficients is less than 3% and 1%, respectively.

Data analysis. For short spin-echo times, Δt, processes like adsorbate vibrations or intra-cell diffusion can be visible in the polarization curves as oscillations and a fast initial drop, respectively. Since we only focus on aperiodic long time scale diffusion, we exclude these processes from the analysis and describe the polarization with an exponential decay, $A\,e^{-\alpha\Delta t} + C$, to extract the decay constant, α. The offset C, for large Δt, is known to be caused by immobile species like surface defects[2]. To ensure that the data is best described by a single exponential, the following procedure is repeated with successively dropped initial data points until the resulting dephasing rate α converges: the Bayesian probability for the data to be represented by a sum of two exponential decays is calculated for pairs of decay constants with the prefactors and static level marginalized. The most probable set of non-negative parameters is taken as starting point for the Levenberg-Marquardt algorithm. The experimental data was throughout best described by a single decay, although simulated intermediate scattering functions may show an additional fast initial decay. The extra decay is a result of the above-mentioned scattering processes not being included in the simulation, which affects the relative amplitudes (prefactors) of the exponentials. The transition point between simulated decays is therefore shifted towards larger Δt compared to the experiment,

where a possible second decay vanishes with the initial drop. The relative amplitudes can be used to rule out that the detected signal originates from vibrations or intra-cell motion[24].

Methods References

29. Farias, D. & Rieder, K.-H. Atomic beam diffraction from solid surfaces. *Rep. Prog. Phys.* **61,** 1575–1664 (1998).

30. Ponder, J. W. TINKER - Software Tools for Molecular Design. (2015). at <http://dasher.wustl.edu/tinker>

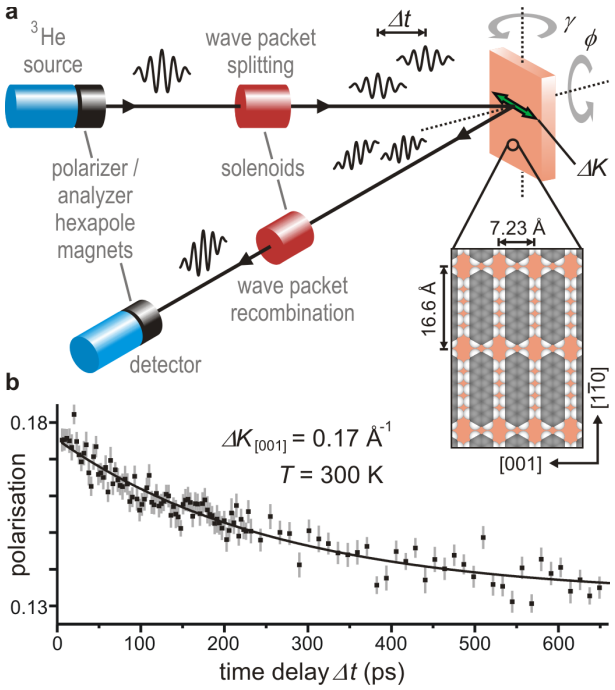

Figure 1 | Measurement principle of helium-3 spin-echo (HeSE). a, A spin-polarized supersonic ^{3}He beam is scattered from the sample surface to probe movement, as explained in the text. Solenoids produce the spin state decomposition (time delay Δt) and recombination. Variation of the incident scattering angle, by rotating γ, determines the surface scattering vector, $\Delta \boldsymbol{K}$, while ϕ sets the probed azimuthal direction (green arrow). The magnified surface scheme shows the pentacene monolayer on Cu(110) in a (6.5 × 2) superstructure with the main symmetry directions and lattice distances. **b**, A typical HeSE measurement of aperiodic diffusion shows an exponential decay in spin polarization with Δt, from which we obtain the decay constant, α. Error bars indicate standard errors of the detected intensity.

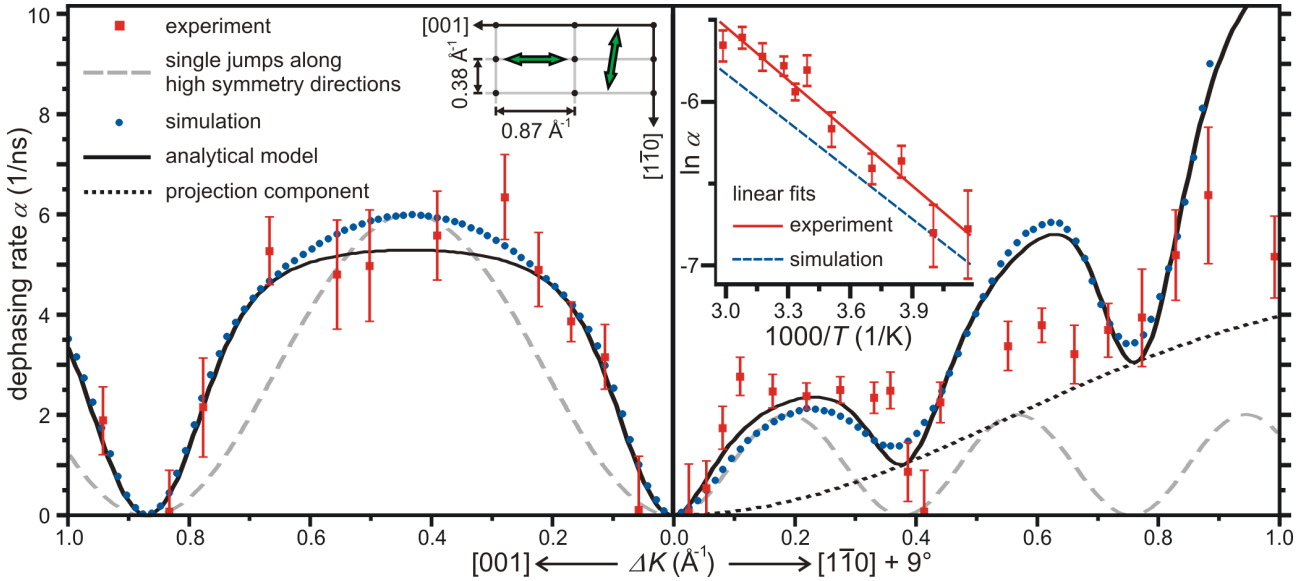

Figure 2 | Dependence of dephasing rate, α, on azimuthal direction and momentum transfer, $\Delta\boldsymbol{K}$. The left- and right-hand panels show the obtained dephasing rate, α, for different momentum transfers along the [001] and 9° off the [1-10] direction, respectively. The associated reciprocal lattice scheme is depicted in the left inset and illustrates the probed directions (green arrows). Experimental data (red squares with error bars, 1σ confidence interval) is shown for a coverage of 0.23 ML deposited onto the pentacene surface and measured at T = 300 K. The simulation (blue circles) agrees with the experimental data. Squared sinusoids (dashed grey lines) are expected for Chudley-Elliot single jump diffusion. Solid black lines illustrate the analytical model. The overall rise (dotted black line) is caused by the small offset angle (see Supplementary Section 2). The rhs inset shows temperature dependent measurements and simulations at $|\Delta\boldsymbol{K}|$ = 0.22 Å^{-1} along the [1-10] + 9° direction which enable an Arrhenius analysis to obtain effective activation energies.

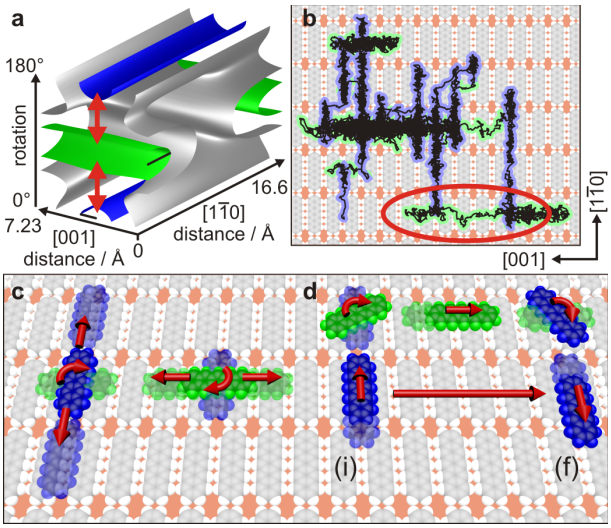

Figure 3 | Simulations result in elementary processes that combine to an apparent long jump. a, Potential energy surface used in simulations consisting of rails (75 meV isosurfaces, green/blue) that are separated by high energy barriers (175 meV isosurface, grey). Transitions between rails require rotation of the molecule (110 meV, red arrows). Note that the rail along [001] is wider, allowing more lateral motion within the rail. Black lines indicate rail half widths. **b**, Simulated trajectory of a single pentacene admolecule (centre of mass) diffusing on the pentacene surface for 9 ns. The molecule is oriented either along [001] (green) or [1-10] (blue) azimuth and mainly moves in the respective direction, interspersed with rotations by 90°. **c**, Single admolecule in potential energy minimum positions and corresponding elementary diffusion processes. Admolecules preferentially move along the direction of their long axis (straight arrows, blue along [1-10], green along [001]) but sometimes turn 90° (curved arrows). **d**, A molecule that (i) initially diffuses along [1-10] until it turns 90°, moves along [001] and finally turns back (f) appears to perform a long jump in the [001] direction (long red arrow, red ellipse in b) covering multiple lattice distances (illustrated is a 6-fold jump).